

**GT2003-38128**

**Unsteady, 3-dimensional flow measurement using a  
miniature virtual 4 sensor Fast Response Aerodynamic Probe (FRAP)**

**Pfau A., Schlienger J., Kalfas A.I., Abhari R.S.**

Turbomachinery Laboratory  
Swiss Federal Institute of Technology  
8092 Zuerich, Switzerland  
pfau@lsm.iet.mavt.ethz.ch

**ABSTRACT**

This paper introduces the new fast response aerodynamic probe, which was recently developed at the ETH Zurich. The technique provides time-resolved, three-dimensional flow measurements using the virtual four sensor technique. The concept and the evaluation of the virtual four sensor probe is discussed in detail. The basic results consist of yaw and pitch flow angles as well as the total and static pressure. They combine to form the unsteady, three dimensional flow vector.

The outer diameter of the cylindrical probe head was miniaturized to 0.84mm, hence probe blockage effects as well as dynamic lift effects are reduced. The shape of the probe head was optimized in view of the manufacturing process as well as aerodynamic considerations. The optimum geometry for pitch sensitivity was found to be a cylindrical surface with the axis perpendicular to the probe shaft. The internal design of the probes led to a sensor cavity eigenfrequency of 44kHz for the yaw sensitive and 34kHz for the pitch sensitive probe.

Data acquisition is done with a fully automated traversing system, which moves the probe within the test rig and samples the signal with a PC-based A/D-board. An error analysis implemented into the data reduction routines revealed acceptable accuracy for flow angles as well as pressures for many turbomachinery flows. Depending on the dynamic head of the application the yaw angle is accurate within  $\pm 0.35^\circ$  and pitch angle within  $\pm 0.7^\circ$ .

In the final section, a comparison of time averaged results to five hole probe measurements is discussed. The advantages of the new probe, beside its unique smallness, are the complete unsteady kinematic information and the improved recording of unsteady total pressure measurement as it is pointed out in a comparison against a 2D virtual three sensor probe.

**NOMENCLATURE**

$C_p$  Pressure coefficient [-]  $C_p = \frac{P - P_{static}}{P_{total} - P_{static}}$   
C Non dimensional circumferential position

d Probe head diameter (0.84mm)  
D Free jet diameter (100mm)  
f Frequency  
K Calibration coefficient  
M Mach number  
p Pressure  
R Non dimensional radial height  
U Voltage  
v Velocity  
 $\phi$  Yaw angle  
 $\gamma$  Pitch angle  
Probe 1 Yaw angle sensitive probe  
Probe 2 Pitch angle sensitive probe  
FRAP Fast response aerodynamic probe

**I. INTRODUCTION**

Unsteady flow measurement technology is indispensable for today's turbomachinery research. Efficiencies in turbomachinery components are high due the effort of research and development during the last century. In order to improve this high standard the research of recent decades concentrated on unsteady flow effects which can be exploited for efficiency increase [9].

One of the established unsteady measurement technologies is the fast response probe based on piezo-resistive miniature silicon sensors. Three review papers on these efforts have been published, recently: Ainsworth et al. [1], Sieverding et al. [11] and Kupferschmied et al. [7]. These papers together give a broad conspectus of the current state of the art. In order to exploit the full frequency band width of the sensors and to reduce influences of Reynolds-number effects, Ainsworth et al. [1] work with flush mounted sensors in a kiel probe head geometry. A new probe concept to avoid wake induced

unsteady perturbations on the pressure signals was developed and brought into operation by Brouckaert [2]. Schlienger et al. [8] demonstrated that pitch angle information can be gained out of five measurements with a single sensor probe of specific elliptical or spherical head design. Using commercial sensors, this is a cost effective way to measure the unsteady total pressure.

With the design and build of the new 2-stage axial research turbine ‘LISA’ [10] a new field of application to the FRAP measurement technology arose, demanding additional requirements due to the nature of investigations.

1) Ability to measure unsteady yaw and pitch angles in a range of  $\pm 20^\circ$  as well as total and static pressure resulting in an unsteady 3d flow vector.

2) Lowest blockage possible for measuring small scale flows, which gives a small measurement volume and is beneficial to dynamic errors in the probe readings.

3) Good frequency response up to the highest expected frequency of the 10th harmonic of 19kHz, as reported i.e. from Busby et al. [3].

## II. CONCEPT, DESIGN AND CONSTRUCTION

### II.1 Measurement concept

The measurement concept is based on the idea of emulating a true four sensor probe with two single sensor probes. In Fig.1 the way both probes work together in tandem is explained. Probe 1 is turned into three positions similar to a virtual three sensor probe. Position 1 is the center position which is close to the total pressure of the flow. Due to the cylindrical surface of the head, p2 and p3 gain yaw angle sensitivity. To derive the pitch angle a fourth measurement is necessary. In a second set up, probe 2 is positioned into exactly the same radial and angular position as probe 1 in position 1. The pressure on the inclined surface p4 compared with the pressure in position 1 results in a pressure difference, which is pitch angle sensitive.

All four pressure signals are brought together in a set of calibration coefficients representing a dimensionless yaw ( $K_\phi$ ) and pitch angle ( $K_\gamma$ ) and total ( $K_t$ ) and static pressure ( $K_s$ ) (see eq.1). The signals must be phase locked to each other by an independent blade or rotor trigger signal. Consequently, the phase locked data sets have to be averaged to gain the deterministic portion of the true unsteady flow. The stochastic portion of the unsteady signal is lost during the averaging procedure.

$$K_\phi = \frac{p_2 - p_3}{p_1 - p_m}; K_\gamma = \frac{p_1 - p_4}{p_1 - p_m}; K_t = \frac{p_{tot} - p_1}{p_1 - p_m};$$

$$K_s = \frac{p_1 - p_{stat}}{p_1 - p_m}, \text{ where } p_m = (p_2 + p_3)/2. \quad (1)$$

By using polynomial calibration models of the dependencies  $\phi(K_\phi, K_\gamma)$  and  $\gamma(K_\phi, K_\gamma)$  the flow angles can directly be derived out of the pressure signals. In a second step total and static pressure are calculated using polynomial calibration models of the form  $K_t(\phi, \gamma)$  and  $K_s(\phi, \gamma)$ .

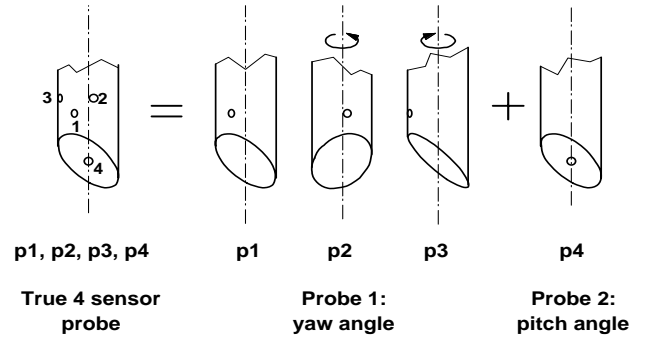


Figure 1: Measurement concept of a virtual 4 sensor probe.

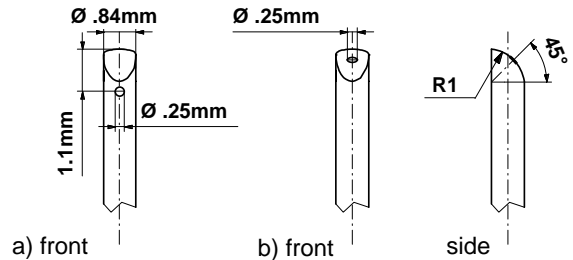


Figure 2: Final probe head design: a) yaw angle sensitive probe, b) pitch angle sensitive probe

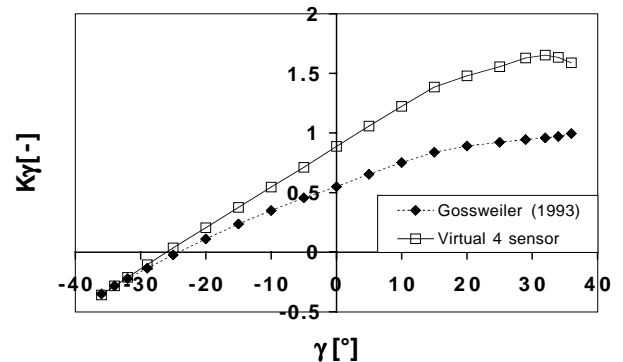


Figure 3: Comparison of calibration coefficient  $K_\gamma$ : Gossweiler [5] and virtual 4 sensor probe,  $\phi=0^\circ$

### II.2 Probe head optimisation and design

To optimize the head design, a pneumatic probe with exchangeable head of 4mm diameter was built. Several head geometries were designed with view on the manufacturing process and tested within the free jet calibration facility of the laboratory [6]. The final design is depicted in Fig.2. The diameter of the curvature was chosen to be 2.4 times the head diameter. The cylinder cuts the head such that it merges

tangentially on the front side of the probe. The hole of the first probe, giving the yaw angle sensitivity, is placed at a distance of 1.1 mm to the tip. The second probe has a hole inclined under 45°, which gives pitch angle sensitivity. The hole to shaft diameter ratio is 0.3.

In Figure 3 the pitch sensitive calibration coefficient at 0° yaw angle is presented. At positive pitch angles around 25° the curve flattens and passes a maximum. The pitch angle sensitivity was found to be 50% higher than in the case of Gossweiler's [5] geometry, which is shown in Fig.1.

### II.3 Manufacturing

The manufacturing technology is based on consequent miniaturization of the probe head components and the sensor packaging. The technology was first developed and applied by Kupferschmied [6] in order to construct a pitot probe. The sensor has the dimensions of 1.6x0.6x0.4mm. The probe head consists of three parts, which are wire eroded. The base part integrates the reference pressure channel and the side walls, which align and protect the sensor. The sensor is glued into it using a soft silicon adhesive. To complete the probe head's outer shape two parts, a long and a short cover, are glued onto the base part. The short cover is made in two different versions: one with a hole on the stem cylinder the other with a hole introduced into the pitch angle sensitive surface. The size of these parts are at 0.84x0.6x0.3mm. A reference pressure tube and wires are connected to the probe head. Tube and wires lie within a shaft of 2.5mm diameter, which connects to the main shaft of 6mm outer diameter. At the end of the shaft a small box containing the amplifier completes the probe.

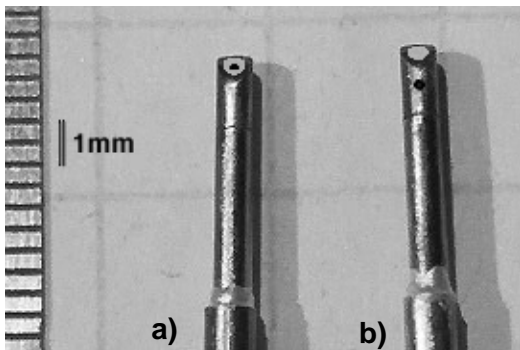


Figure 4: a) Pitch angle sensitive probe, b) Yaw angle sensitive probe

Altogether, an estimated 40 different mechanical and micro-mechanical steps of several hours each are necessary to build one probe. Each step is followed by a hardening time of at least 6 hours. This sums up to 500 hours of elapsed time per probe. The finished pair of probes is presented in Fig.4.

## III. PROBE SUB SYSTEMS AND CALIBRATION

### III.1 Sensors

The pressure sensors working principal is the Wheatstone

bridge. The bridge is fed by a constant current source of 1mA. The excitation voltage  $U_e$  and the signal voltage  $U$  are amplified by the factor of 100 and measured. Thereby, the excitation voltage is a measure for the membrane temperature and the signal voltage is proportional to the differential pressure across the membrane. The sensors, which were built into the probes, have a sensitivity of 8.1mV/mbar for probe 1 and 7.8mV/mbar for probe 2 after amplification.

Each sensor needs to be calibrated individually. The calibration procedures described in Kupferschmied [6] were applied in this case. To derive a sensor calibration model the probe head is exposed to a constant temperature air stream of low velocity (5m/s) within a calibration oven. The temperature steps chosen for this calibration were 15, 25, 35, and 45°C. Each temperature plateau was held for at least 4 hours to ensure temperature equilibrium. During each temperature step pressure cycles of 6 different levels were applied to the reference pressure tube. The pressure range covered by this calibration was 2 to 45kPa. The gathered data is interpolated using a 2 dimensional polynomial in order to get the relationship of voltages to pressure  $p(U, U_e)$  and temperature  $T(U, U_e)$ .

The sensors used here are affected by a time dependent offset drift of the signal  $U$  while the excitation voltage  $U_e$  stays relatively constant with time. The drift affects the offset of the sensor but not its sensitivity. To account for the effect of drift the offset of the sensor must be known during measurements with the probes. Therefore, an adjustment procedure is applied to the probes before and after each measurement task. The probes must be brought into an environment, where the pressure at the probe tip is known. This can be achieved by pulling the probe out of the flow regime into a settling chamber where the fluid is at a rest and the static pressure can be measured. Then two pressure levels are applied to the reference pressure tube and  $U$  and  $U_e$  are measured. The resulting two adjustment coefficients affect the offset and the gain of the sensor model.

An additional undesirable behavior of the piezo-resistive sensor is the effect of self heating. If the air around the probe head is at a complete rest the heat produced in the sensor is not convected away. This leads to a higher sensor membrane temperature and therefore also to a higher temperature reading of the probe ( $U_e$ ). Investigating this effect it was found that a velocity step from 5m/s to 0m/s and back to 5m/s resulted in a temperature change in both step directions of 2°C. This implies that good quantitative steady temperature measurements are difficult to achieve for flow in stagnating regions.

The accuracy of pressure evaluation was found to be  $\pm 20$ Pa for both probes covering the pressure range of application 0 to 30kPa, which equals to 0.07% FS. This result was also found

to be true across velocity step of 5 to 0m/s and back where all velocity conditions were kept constant for one hour.

### III.2 Steady aerodynamics

The steady aerodynamic behavior of the probe determines the calibration range in yaw and pitch angle. The free jet probe calibration facility used for the calibration is described by Kupferschmied [6] allowing a yaw angle variation of  $\pm 180^\circ$  and pitch angle variation of  $\pm 36^\circ$ .

In Figure 5 the non-dimensional pressure readings of both probes for varying yaw angle at a constant pitch angle of  $0^\circ$  are depicted for two Mach-numbers, 0.15 and 0.3. For the yaw angle sensitive probe 1  $C_p$  becomes 0 at a turning angle of  $\pm 45^\circ$ . These positions were chosen to measure positions 2 and 3 in the measurement concept (see also Fig.1). Changes in pressure distribution due to Mach-number variations are small. The Reynolds-number based on the head diameter is  $Re_d=2400$  at the lower and  $Re_d=4800$  at the higher Mach-number. This is well within the subcritical range of  $10^3$  to  $10^5$  where the drag coefficient of the probe head stays constant. Therefore, any viscosity effects on the probe head can be omitted for a range above a Mach number of 0.06.

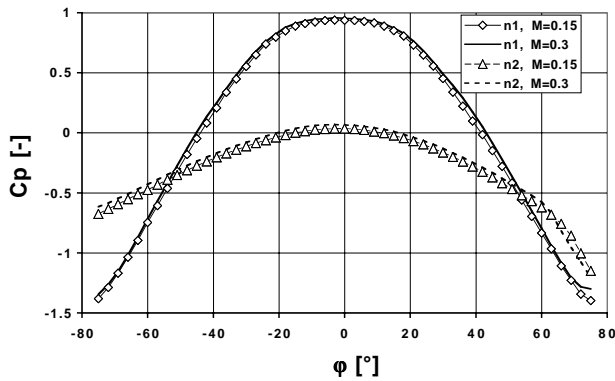


Figure 5: Pressure reading of both probes:  $\gamma=0^\circ$ ;  $M=0.15, 0.3$

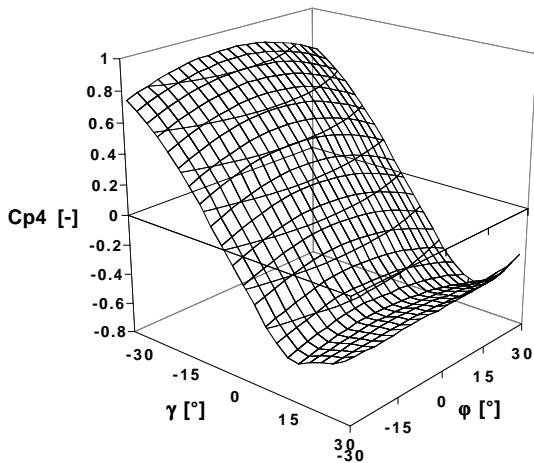


Figure 6: Non-dimensional pressure  $C_{p4}$ ,  $M=0.3$

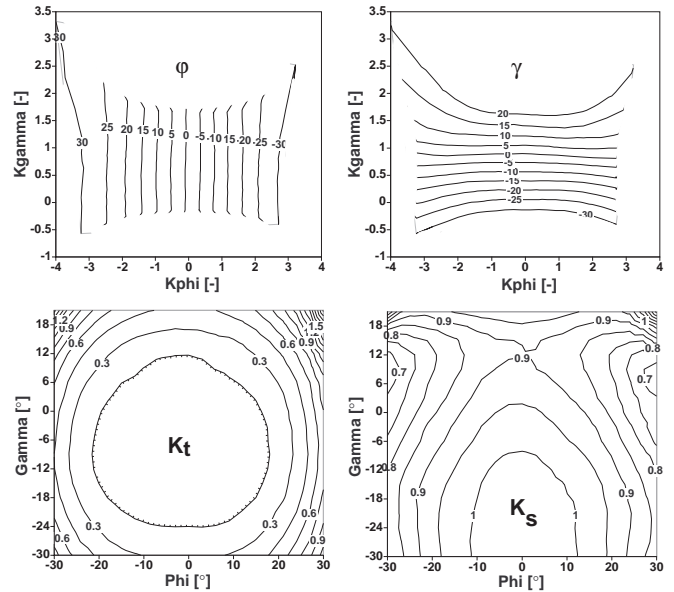


Figure 7: Aerodynamic calibration surfaces:  $\phi$ ,  $\gamma$ ,  $K_t$ ,  $K_s$

The set of calibration data was taken on an equidistantly spaced grid covering  $\pm 30^\circ$  in yaw and pitch angle. The chosen mesh width of  $3^\circ$  results in  $21 \times 21$  points. The data was non-dimensionalised to correct for the change in atmospheric pressure. Since positions 2 and 3 are shifted by  $45^\circ$  and  $-45^\circ$  respectively, the absolute range of probe yaw angle positions to calculate  $C_{p2}$  and  $C_{p3}$  are  $15^\circ$  to  $75^\circ$  and  $-75^\circ$  to  $-15^\circ$ . The pressure distribution of position 4 is shown in Fig.6, which shows, that pitch angle sensitivity is decoupled from yaw angle position. Like in Fig.3 the non-dimensional pressure flattens for pitch angles around  $24^\circ$ .

In order to get a working aerodynamic model, the calibration range had to be limited in positive pitch angle direction to  $21^\circ$ . For values higher than  $21^\circ$  the results of the angle evaluation would be ambiguous due to the flattening of the  $C_{p4}$  distribution, see Fig.6. Therefore, the calibration limits can be given to  $\pm 30^\circ$  in yaw and  $-30^\circ$  to  $21^\circ$  in pitch angle. In Figure 7 the calibration surfaces are shown. The lines of constant  $\phi$  and  $\gamma$  in Fig.7a and b are normal to each other, which shows the desired decoupling of both calibration coefficients  $K_\phi$  and  $K_\gamma$ . Only in the corners of the calibration range does the orthogonality get distorted. That is also the region where the highest residuals in the polynomial interpolation occur. The yaw and pitch angle sensitivity defined as  $(\partial K_\phi)/(\partial \phi)$  and  $(\partial K_\gamma)/(\partial \gamma)$  at  $\phi=0^\circ$  and  $\gamma=0^\circ$  are 0.09 and 0.032, respectively. For  $K_t$  values around 0 are expected. In the extremes of the calibration range  $K_t$  becomes as high as 1.8. In most parts  $K_s$  shows values around 1.

With eq.1 all calibration coefficients are defined. According to the  $C_p$  definition,  $C_{p\text{tot}}$  and  $C_{p\text{stat}}$  have values of 1 and 0, respectively. To get the mathematical representation of the

calibration the coefficients are interpolated by using 2 dimensional polynomial of 6th order for the flow angles and 4th order for total and static pressure coefficients. The polynomial coefficients are found by using the least square method. The resulting functions are  $\varphi(K_\varphi, K_\gamma)$ ,  $\gamma(K_\varphi, K_\gamma)$  and  $K_t(\varphi, \gamma)$ ,  $K_s(\varphi, \gamma)$ .

In order to account for blockage effects within the free jet a static pressure correction was applied to the  $K_s$  surface. A cylindrical probe causes a static pressure increase in the measurement plane due to a widening of the jet. Wyler [13] gives a static pressure correction for cylindrical probes in free jets as:

$$\frac{\Delta p}{P_{tot} - P_{stat}} = \frac{2(1.15 + 0.75(M - 0.2))d}{\pi(1 - M^2)D} \quad (2)$$

The ratio of diameters  $d/D$  assumes a probe shape of constant diameter within the jet. This is not the case for this probe since the diameter increases in steps from 0.84 mm to 2.5mm from the center of the jet to its outer radius. Therefore, an equivalent diameter of the probe shaft was used, such that the wetted area within the jet stays constant. For this probe the equivalent diameter is 2mm. At a Mach number of 0.3 the correction becomes 100Pa.

Equation 2 is only valid if the probe shaft is perpendicular to the flow. For the virtual four sensor probe a pitch angle dependent correction is necessary. This was achieved in using Wyler's correction for the zero pitch angle case as the maximum correction. Pitching the probe leads to less blockage area and therefore a smaller correction has to be applied. In order to get the reduction the wetted area within the measurement plane was calculated and set into ratio to the full area. With that the values of  $K_s$  were corrected for pitch angles  $-6$  to  $9^\circ$ . For pitch angles out side this range the correction values became negligible. The correction for positive pitch angles is higher because the recirculation zone behind a body also contributes to the blockage effect.

### III.3 Frequency response

Two different aerodynamic effects influence the frequency response of a FRAP probe. The pneumatic cavity between the pressure tap and the sensor membrane is one source of influence. Associated with the characteristic length of the cavity is an acoustic resonance, which causes higher amplitudes and shifted phase of the signal. The other stems from the fact that probes are intrusive to the flow, resulting in a distortion of the flow field at the location of measurement. The von-Karman vortex street downstream of a cylindrical body can also affect the measurements at the probe tip. In addition to these aerodynamic effect, mechanical vibrations of the probe shaft might alter the frequency response of the probe. The mechanical eigenfrequency of the sensor membrane is very high (around 500kHz Gossweiler [5]) and therefore plays

no role in this type of application.

### Pneumatic eigenfrequency

An estimate of the eigenfrequency of both pneumatic cavities was obtained in the free jet. The total pressure disturbances within the core of the jet were sufficient to acoustically excite the cavity. The free jet was running at a Mach-number of 0.3. In order to have the same kind of excitation for both probes, both probes were positioned such that the holes were facing the flow. The result of these measurements is given in Fig.8.

In the right part of the diagram the eigenfrequencies of both pneumatic cavities are present: 44kHz for probe 1 and 34kHz for probe 2. Both values are close to the eigenfrequency of the miniature pitot described by Kupferschmid [6], which is 46kHz. The larger cavity of probe 2 due to the internal design is reflected in the lower eigenfrequency.

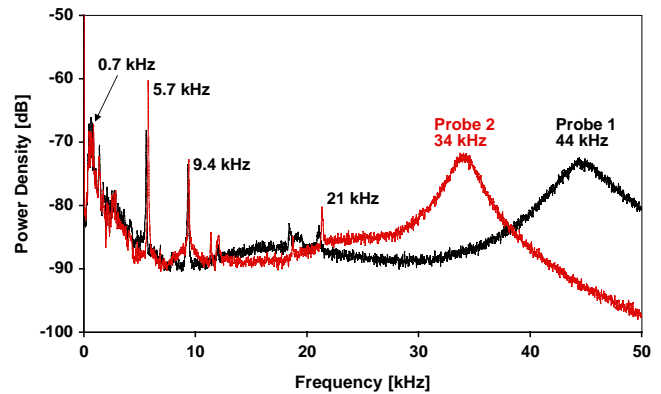


Figure 8: FFT analysis of Probe 1 and 2: free jet core

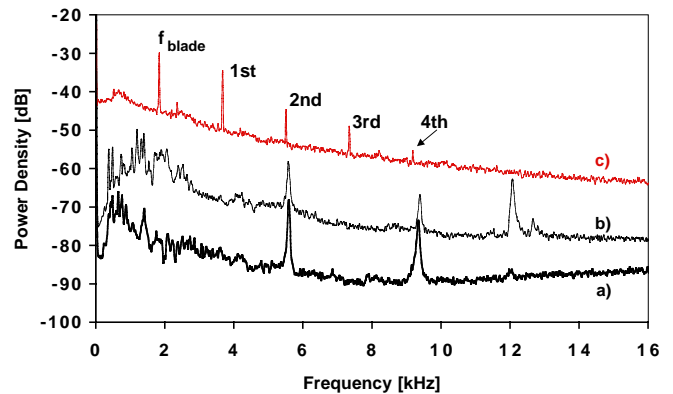


Figure 9: FFT analysis of probe 1: a) Free jet M=0.3, b) Free jet M=0.5, c) LISA stator exit at mid span

### Mechanical vibrations

The FFTs of both probes given in Fig.8 also reveal mechanical vibrations of the shafts due to aerodynamically induced forced response. For probe 1 and 2 two sharp peaks occur having frequencies of 5.7kHz and 9.7kHz. The two peaks could be identified being the eigenfrequencies of the

probe head itself and the second shaft. Increasing the Mach number from 0.3 to 0.5 does not alter those frequencies as shown in Fig.9.

Using the probe within the turbine test rig the mechanical vibrations were not detected as can be seen in Fig.9. The probe was mounted downstream of the second stator as indicated in Fig.11, with the tip at mid span position. The Mach-number there is around 0.35. The blade passing and the higher harmonics up to the fourth order are present. No further significant frequencies are found.

For the present application a correction of the pressure signal of the probes based on a transfer function is not considered necessary. The highest frequency present in the test rig, 10kHz, is well away from the first rise in amplitude at 30kHz. For frequencies lower than 25kHz no change in amplitude and phase is expected.

### Dynamic effects

The reduced frequency as given in eq.3 is a non-dimensional measure for the probe's response to excitation frequencies:

$$k = \frac{fd}{v} \quad (3)$$

For this application two characteristic flow regimes have to be investigated. Downstream of the rotor, flow velocities range up to 35m/s; downstream of the stator velocities are higher up to 120m/s. With a blade passing frequency of 1890Hz the reduced frequency of the probe becomes 0.045 and 0.013 for the two characteristic velocities. Gizzi [4] suggested a limit of  $k > 0.1$ , above which corrections on dynamic probe measurements become necessary. Both flow regimes are well below the critical reduced frequency due to the miniature dimensions of the probe head.

The miniature size of the probe is also beneficial to the characteristics of the von-Karman vortex street. The shedding frequency is given by the Strouhal-number which becomes 0.2 for the range of Reynolds-number. The two flow regimes within the test rig have an accompanying shedding frequency of 8.3kHz for the lower and 28.5kHz for the higher velocity.

### III.4 Error Analysis

The error calculation was implemented directly into the evaluation program whose structure follows Fig.10. It is based on the error propagation eq.4 and follows the scheme of Treiber et al.[12].

$$\Delta F = \pm \sqrt{\left(\frac{\partial F}{\partial x} \cdot \Delta x\right)^2 + \left(\frac{\partial F}{\partial y} \cdot \Delta y\right)^2 + \dots} \text{ with } F=f(x,y,\dots) \quad (4)$$

Starting point of the error calculation was the differential pressure measured with the sensors. The process of evaluating the sensor voltages, including the offset and gain correction

coefficients  $J_1$  and  $J_2$ , was found to be accurate to within  $\pm 20\text{Pa}$  against a first order accurate pressure measurement device. A list of resulting uncertainties is given in Tab.1. Two characteristic cases, the flow downstream of a rotor ( $M=0.1$ ) and the flow downstream of a stator ( $M=0.35$ ), were investigated. A higher dynamic head is of course beneficial to the absolute accuracy of the flow angles, as the calibration coefficients are inversely proportional to the dynamic head. The total pressure is less accurate than the static pressure since the residuals of the polynomial model are higher and contribute to the error. One possibility to achieve a lower error would be to partition the calibration surface in additional areas. With that, the polynomial approximation would get closer to the points of calibration values. Another possibility would be to use polynomial calibration models of the form  $K_r(K_\phi, K_\gamma)$  and  $K_s(K_\phi, K_\gamma)$ , which would reduce the overall error of total and static pressure caused by the propagation of the error in flow angle. For the Mach-number a relative error of 1.2% and 2.5% respectively is found.

Parameters	M=0.1	M=0.35
$\phi$	$\pm 1^\circ$	$\pm 0.35^\circ$
$\gamma$	$\pm 2^\circ$	$\pm 0.7^\circ$
$C_{ptot}$	$\pm 0.0025$	$\pm 0.0033$
$C_{pstat}$	$\pm 0.0012$	$\pm 0.0022$
$p_{tot}$	$\pm 80\text{Pa}$	$\pm 120\text{Pa}$
$p_{stat}$	$\pm 60\text{Pa}$	$\pm 85\text{Pa}$
<b>M</b>	<b><math>\pm 2.5\%</math></b>	<b><math>\pm 1.2\%</math></b>

**Table 1:** Typical error band width of flow parameters

Looking at the relative accuracy of the local dynamic head downstream of the stator the errors of total and static pressure add up to 3.5% of dynamic head. Downstream of the rotor this error becomes 12% of dynamic head. At even lower Mach numbers the measurement accuracy becomes less. Experience shows that the lowest Mach number at which the probe is still giving in that sense reasonable data is  $M=0.06$ .

## IV. PROOF OF CONCEPT

### IV.1 First measurements and data reduction

The results presented in this section stem from a first measurement campaign within the two-stage, axial turbine 'LISA'. The measurement plane was positioned downstream of the second stator in mid axial position between stator trailing edge and rotor leading edge, as indicated in Fig.11. The circular arrow depicts the sense of rotation. The test rig was running at design operation point and the tip clearance was set to 0.36% of blade span.

The measurements with the yaw angle sensitive probe were performed first followed by the pitch sensitive probe. The mounting procedure for both probes is repeatable in the order of  $\pm 0.1\text{mm}$  in radial extent and  $\pm 0.05^\circ$  in turning angle. Twenty-one circumferential positions per blade pitch were measured where an accuracy of  $\pm 0.05\text{mm}$  was ensured by an encoder.

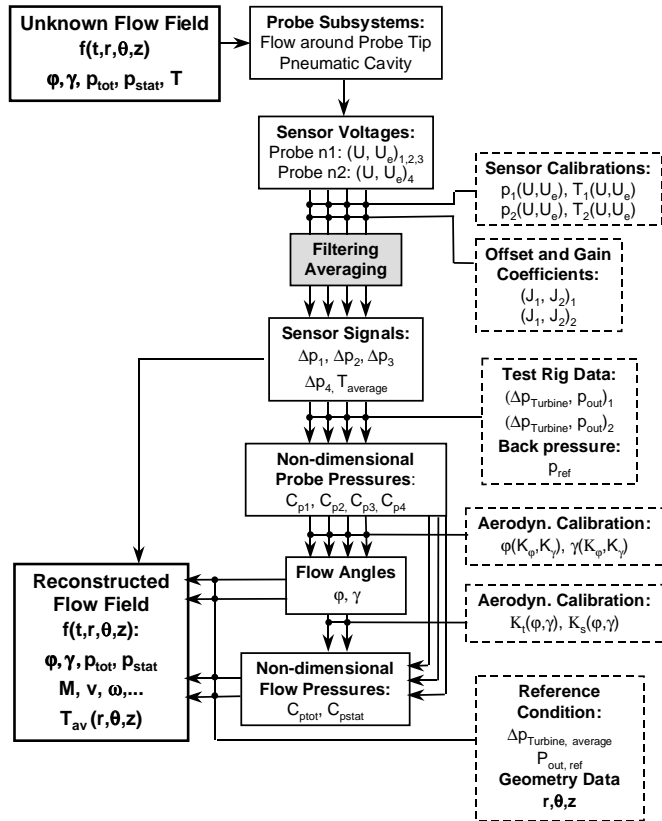


Figure 10: Signal paths from flow to measurement results

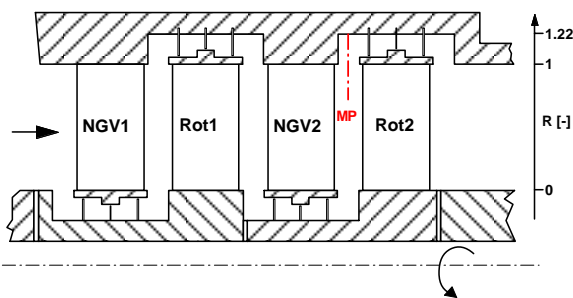


Figure 11: Cross section of the test turbine indicating the measurement position

The measurement task files run as radial immersions into the flow field taking three turning angle positions ( $0^\circ, \pm 45^\circ$ ) at each radial position for the yaw angle sensitive probe and the  $0^\circ$  angular position for probe 2. The measurement locations range from cavity floor to the secondary loss core of the stator tip end wall flow, which is located at 75% span. In general 16

measurement position were applied in radial direction. Before and after each radial traverse the offset and the gain of the sensors were measured by applying two pressure levels to the reference pressure tube. Each measurement position is sampled 3 seconds at a rate of 200kHz which results in 13 Gbytes of raw data per measurement plane.

In a first step of the data processing, 100 data sets phase-locked to one specific trigger position on the rotor circumference are cut out of the raw data and saved in a file. Each resulting data set covers three consecutive passages at 106 samples per passage. To this raw signal the calibration model with the sensor adjustment coefficients is applied, providing the differential pressure and absolute temperature of the sensor. The pressure data is filtered using a zero-phase digital filtering algorithm, see Fig.10. The filter characteristic is a 7th order Butterworth filter of 15 kHz cut off frequency. The filtered pressure signals then are phase lock averaged and made non dimensional resulting in the pressure coefficient given in the nomenclature. Applying the aerodynamic calibration model the flow angles as well as total and static pressure are derived, which allows for further flow quantities like absolute or relative Mach-number, and velocity components.

## IV.2 Comparison to five hole probe data

In Figure 12 the non-dimensional, time averaged total pressure measured with the virtual four sensor probe and the pneumatic five hole probe data are brought together. The direction of view is upstream onto the trailing edge of the stator. The dashed line depicts the tip radius of the main flow annulus. The cavity floor has a radial height of 1.22.

Both probes capture the basic steady flow phenomena including the loss core at 75% radial height, which is connected to the wake at lower radii. Secondly, the strong total pressure gradient of a shear layer, which connects the cavity flow to the main flow, is found in both cases at a radial height of 95%. The shapes of the total pressure contours are virtually the same, which indicates a good agreement between the measurement techniques.

Three parameters define the flow besides the total pressure: the flow angles and the static pressure. Figure 13 gives the pitch-wise averaged difference between the results of both measurement technologies. Fig.13a shows differences of yaw angle of  $\pm 1^\circ$ , which is considered to be a good agreement. The pitch angle difference ranges  $-3^\circ$  to  $0.5^\circ$ . This is consistent with Tab.1, which shows, that errors in pitch angle are expected to be twice as large as the ones in yaw angle. Within the cavity the difference in pitch angle is negative. End wall proximity effects or blockage effects might be the reason for this. Both flow angles show a change in difference close to the tip radius, where the shear layer is located. High total pressure gradients induce an error in the flow angle readings, which

might reach up to  $\pm 0.5^\circ$  for both types of probes.

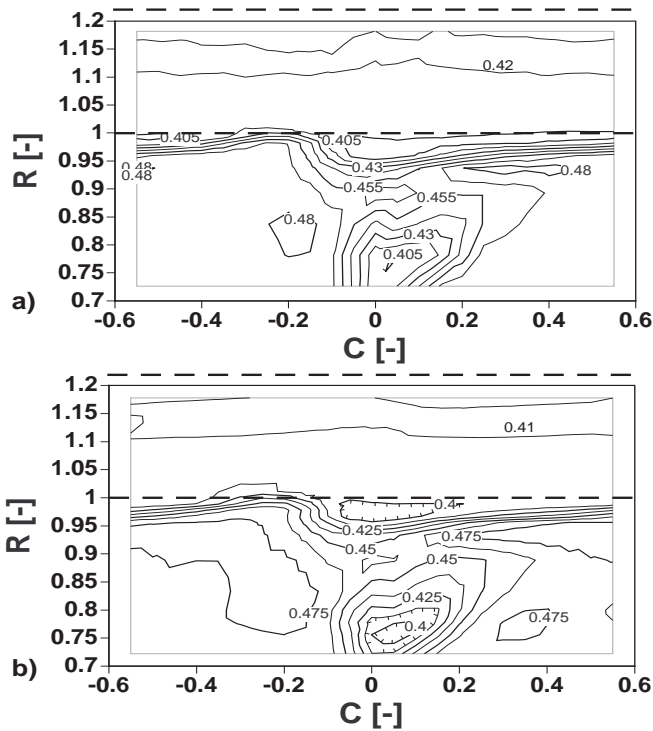


Figure 12: Comparison of non dimensional total pressure: a) virtual 4 sensor probe, b) 5 hole probe

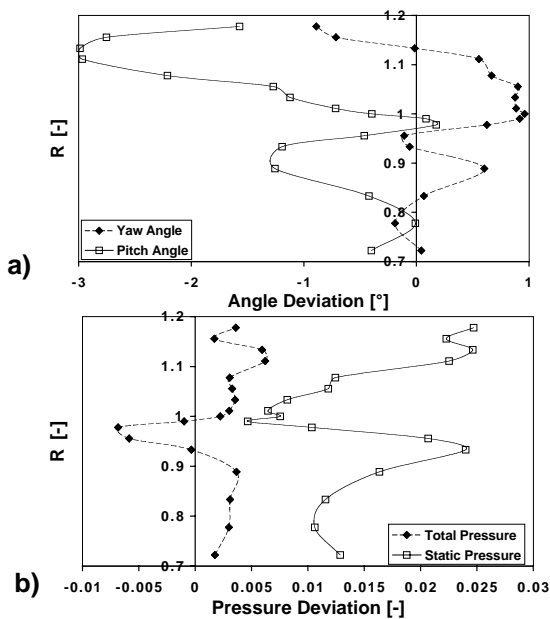


Figure 13: Pitch-wise averaged differences of V4SS time averaged and 5 hole probe results: a) flow angles, b) non-dimensional pressures

The difference in non-dimensional total and static pressure measurement is presented in Fig.13b. Both measurement technologies measure the total pressure in good agreement. The level of deviation ranges around 0.002 in most parts of the

span. In the region of high total pressure gradient around  $R=1$  the difference gets negative. Concerning the average static pressure level, the virtual four sensor probe gives a 0.018 higher non-dimensional static pressure than the five hole probe.

### IV.3 Comparison of 2D versus 3D unsteady measurements

In order to show the capability of resolving unsteady flow structures, the unsteady results are compared to measurements taken with a single sensor FRAP probe running in a virtual three sensor mode. This probe has a head diameter of 1.8mm and measures two dimensionally, as described in Kupferschmied [6].

A comparison of distance-time diagrams of both probes downstream of the second stator is given in Fig.14. It shows the non dimensional total pressure at mid span position downstream of the second stator. Note, that the color legend is not the same for both diagrams. The thick dashed line marks the non dimensional circumferential position of the wake.

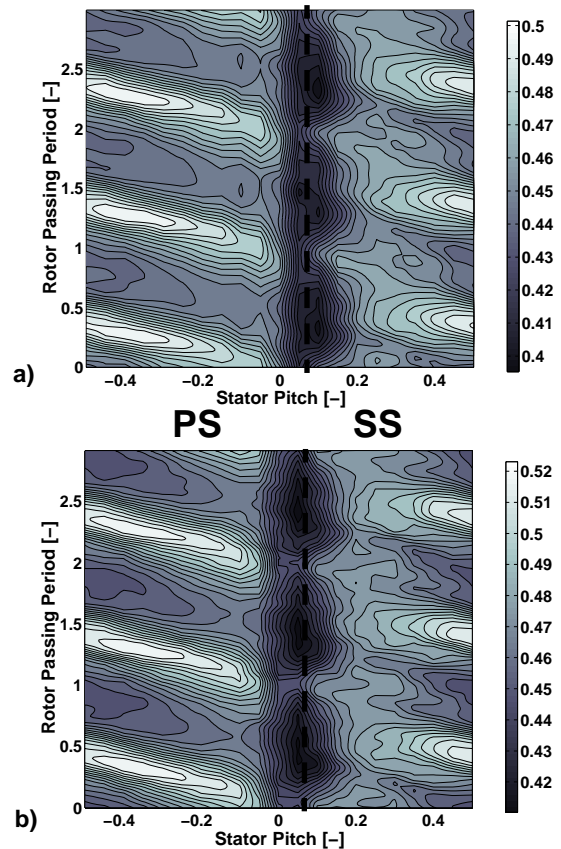


Figure 14: Circumference-time-diagram of non dimensional total pressure at mid span of stator exit: a) single sensor FRAP, b) virtual four sensor FRAP

The dominating feature in this way of displaying unsteady data are inclined iso-lines which express convected flow

features, e.g. wakes of the upstream rotor. At  $C=-0.5$  and  $+0.5$  periodicity in time and space is proven for both measurement technologies. Now consider a circumferential position of  $+0.3$ . Moving upward sound flow with a high non dimensional total pressure of 0.5 is alternating with wakes of the upstream rotor showing a lower total pressure of 0.45. Both probes capture this effect in level and shape and therefore agree well in that area of the flow.

At the wake center line a difference in the time response is obvious. The unsteady behaviour of the wake measured with the virtual four sensor is a periodic opening and contraction in time symmetrically to the wake center line. The same flow measured with a single sensor probe, however, looks different: the symmetry is lost, i.e. on the pressure side of the wake no opening and contraction can be observed. At the same position the pitch angle shows high negative values (not shown in a figure). Obviously, the third dimension contributes substantially to the total pressure and can not be neglected.

## V. CONCLUSIONS

A novel miniature fast response aerodynamic probe (FRAP) has been developed, built and tested. It is based on the measurement concept of a virtual four sensor probe. It can measure three dimensional and unsteady flow up to frequencies of 25kHz covering flow angles of  $\pm 30^\circ$  in yaw and  $-30^\circ$  to  $+21^\circ$  in pitch direction. The unique miniature size of the probe of 0.84 mm diameter is a necessity for the use of the probe in small scale flow. In comparing the results against a miniature pneumatic five hole probe with hook shaped head the measurement concept was proven to be applicable. With the comparison against a 2D unsteady measurement technique it is pointed out that accounting for the third dimension not only completes the view of the kinematic flow field but also improves the total pressure measurement. With this probe a new useful measurement technique is at hand to study the 3D unsteady flow field.

## ACKNOWLEDGMENTS

We would like to extend our thanks to P. Kupferschmied who shared his knowledge on probe manufacturing. Without an excellent technical support, in particular T. Künzle, this probe would not have been possible.

The flow measurements in the turbine were supported by the German Federal Ministry of Economy (BMWI) under file numbers 0327060D and 0327060F. The authors gratefully acknowledge AG Turbo, Alstom Power and Rolls-Royce Germany for their support and permission to publish figures of the flow field in this paper

## REFERENCES

[1] Ainsworth, R.W., Miller, R.J., Moss, R.W., Thorpe, S.J., 2000, "Unsteady pressure measurement", Measurement Science Technology, Vol.11, p1055-1076

[2] Brouckaert, J.F., 2000, "Development of single- and multi-hole fast response pressure probes for turbomachinery application", Proc. of the 15th Symp. on measuring techniques in cascades and turbomachines, Florence, Italy

[3] Busby, J.A., Davis, R.L., Dorney, D.J., Dunn, M.G., Haldeman, C.W., Abhari, R.S., Venable, B.L., Delaney, R.A., 1999, "Influence of vane-blade spacing on transonic turbine stage aerodynamics: Part II-Time-resolved data and analysis", J. of Turbom., Vol. 121 No.4, pp673-682

[4] Gizzi, W., 2000, "Dynamische Korrekturen für schnelle Strömungs sonden in hochfrequent fluktuierenden Strömungen", ETH diss. No. 13482, Zurich, Switzerland

[5] Gossweiler, C., 1993, "Sonden und Messsystem für schnelle aerodynamische Strömungsmessung mit piezoresistiven Druckgebern", ETH diss. No. 10253, Zurich, Switzerland

[6] Kupferschmied, P., 1998, "Zur Methodik zeitaufgelöster Messungen mit Strömungs sonden in Verdichtern und Turbinen", ETH diss. No. 12774, Zurich, Switzerland

[7] Kupferschmied, P., Köppel, P., Gizzi, W., Roduner, C., Gyarmathy, G., 2000, "Time-resolved flow measurements with fast-response aerodynamic probes in turbomachines", Measurement Science Technology, Vol.11, p1036-1054

[8] Schlienger, J., Pfau, A., Kalfas, A.I., Abhari, R.S., "Single pressure transducer probe for 3D flow measurements", Proc. of the 16th Symp. on measuring techniques in cascades and turbomachines, 2002, Cambridge, UK

[9] Schulte, V., Hodson, H.P., 1998, "Prediction of the becalmed region for LP turbine profile design", J. of Turbomachinery, Vol. 120, No. 4, pp 839-846

[10] Sell, M., Schlienger, J., Pfau, A., Treiber, M., Abhari, R.S., 2001, "The 2-stage axial turbine test facility LISA", Proc. ASME Turbo Expo, 2001-GT-492, June 4-7, New Orleans

[11] Sieverding, Ch., Arts, T., Denos, R., Brouckaert, J.F., 2000, "Measurement techniques for unsteady flows in turbomachines", Exp. in Fluids, Vol. 28, No.4, pp 285-321

[12] Treiber, M., Kupferschmied, P., Gyarmathy, G., 1998, "Analysis of the error propagation arising from measurements with a miniature pneumatic 5-hole probe", Proc. of the 13th Symp. on measuring techniques in cascades and turbomachines, 1998, Limerick, Ireland

[13] Wyler, J.S., 1975, "Probe blockage effects in free jets and closed tunnels", Vol.10, pp 509-515, J. of Engineer. for Power